# Radiometric Normalization of SPOT-5 Scenes: 6S atmospheric Model versus Pseudo-invariant Features

Aurélie Davranche, Gaëtan Lefebvre, Brigitte Poulin

**RADIOMETRIC NORMALIZATION OF SPOT-5 SCENES:**
**6S ATMOSPHERIC MODEL VS. PSEUDO-INVARIANT FEATURES**

**Short title**: Radiometric normalization of SPOT-5 scenes

**Description**: The 6S code provides a significantly lower radiometric variation (2.8%) than the use of pseudo-invariant features (4.1%), which remains a valid approach with only a few carefully selected invariant sectors.


## Abstract

We compared the efficiency and robustness of two radiometric correction techniques applied to six SPOT-5 scenes used for assessing environmental changes of Camargue wetlands: the 6S atmospheric model and 86 pseudo-invariant features (PIFs) found in deep water, pine trees, roofs and sand. The few PIFs were selected subjectively following the low number of potentially invariant sectors available on the scenes. Both approaches provided a similar radiometric variation (6S =4.3%; PIFs = 4.0%). The latter increased from water to pine trees, to roofs and sand, with five reference points per feature being identified as cost effective. The withdrawing of variant features among the PIFs across dates or points caused a significant decrease in radiometric variation, especially with 6S (6S = 2.8%, PIFs = 3.4%). As many as 31 point per type of PIFs would be necessary to provide a radiometric variation that is not significantly different from that obtained with 6S, whereas nearly 300 and 4000 points per feature would be required to provide similar or better results than the 6S code, respectively. Use of a few PIFs remains a valid approach, as long as the invariant sectors cover a wide range of

brightness and are represented by objects of which the radiometric variation has preliminarily been tested.

Keywords: 6S atmospheric model, pseudo-invariant features, radiometric normalization, SPOT-5 scenes, wetland monitoring, Camargue, FRANCE

**Introduction**

The Camargue or Rhône Delta in southern France includes 90 000 ha of natural habitats, mostly temporary marshes used for various traditional and socio-economic activities (waterfowl hunting, reed harvesting, cattle grazing) of which the hydrological functioning is increasingly man-made to improve economic yield (Mathevet, 2004). The input of freshwater in these brackish marshes and the modification of their hydroperiod through the year influence their floristic composition and vegetation biomass, justifying a follow up of their management and health state (Tamisier and Grillas, 1994). Two third of these marshes are located outside protected areas on relatively small private estates. This fragmented configuration within a large geographical area makes monitoring based on repeated ground measures difficult. The potentialities of remotely sensed imagery for monitoring the environmental changes of these marshes are being assessed with time series of SPOT-5 scenes, which provide a multispectral mode with four bands: green (B1: 0.50 – 0.59 µm) , red (B2: 0.61 – 0.68 µm), near infrared (B3: 0.79 – 0.89 µm), and short-wave infrared (SWIR: 1.58 – 1.75 µm). The first three bands yield a 10-m resolution, and the SWIR band can be resampled to 10 m from the original 20-m resolution (SPOT Image, 2005). The analysis of multitemporal images requires a calibration of their digital counts to common reference values, because their radiometry is affected by solar illumination angles, view angles, atmospheric conditions, reflectance anisotropy, and sensor calibration trends, all of which potentially vary across images (Lillesand and Kiefer, 2000; Schott, 2007).

Among the several methods of radiometric normalization available (see Furby and Campbell, 2001 for a review) is the use of pseudo-invariant features (PIFs) (Schott et al., 1988, Caselles and Lopez Garcia, 1989; Eckhardt et al., 1990; Paolini et al., 2006; Schroeder et al., 2006). This relative approach does not eliminate the effect of the atmosphere, but allows one to calibrate all images to a similar atmospheric state from one image used as a reference. Features presumed to have constant reflectance over time are manually or statistically selected on the image to cover the full range of spectral brightness values. It does not require data other than the image itself, but the reference image (date) must be selected carefully to maximise the constancy of the corrections. It should (i) be cloud-free; (ii) have a relatively clear atmosphere; (iii) contain data within the storage format range for all bands; (iv) represent a time of year appropriate for the application; and (v) have the best possible dynamic range (Furby and Campbell, 2001). A small look angle will further minimize the amount of atmospheric attenuation and haze on the image (Eckhardt et al., 1990). Size of invariant targets should be adapted to the ground resolution of the sensor and cover several pixels to avoid mixed-pixels effects (Schott et al., 1988). According to Eckhardt et al. (1990), the PIFs should (i) be approximately located at the same elevation so that the thickness of the atmosphere over each target is similar; (ii) contain only minimal amounts of vegetation to reduce change in spectral reflectance over time; (iii) be located in relatively flat areas so that changes in sun angle between images will produce the same proportional increases or decreases in insolation; (iv) not exhibit changes in their spatial pattern, and (v) have a wide range of brightness values for the regression model to be reliable. Although the type of invariants targets and the number of points used will affect the accuracy of the normalization, these limitations have rarely been quantitatively addressed.

Application of a radiative transfer model based on generalised atmospheric conditions is another approach for radiance normalization (Richter, 1990; Tanré et al., 1990; Rahman and Dedieu, 1994; Vermote et al., 1997). These numerical atmospheric transmission codes provide an absolute correction, but generally require measurements of atmospheric constituents to be taken simultaneously with the acquisition of the image. Although originally difficult to apply by the non-physicist geographers, these codes have been simplified in their application (Richter, 1990; Rahman and Dedieu, 1994; Kergomard, 2000). Moran et al. (1992) tested atmospheric correction procedures under a variety of atmospheric conditions including radiative transfer codes like the Simulation of the Satellite Signal in the Solar Spectrum or 5S (Tanré et al., 1990), and concluded that they were successful in reducing the error of reflectance estimation even when they were used with estimates of atmospheric correction instead of the atmospheric optical depth measurements on the site. The Second Simulation of the Satellite Signal in the Solar Spectrum (6S) is an improved version of 5S, developed by the Laboratoire d'Optique Atmosphérique (Université des Sciences et Technologies de Lille, France). This widely used atmospheric radiative transfer code, developed by Vermote et al. (1997), predicts the sensor signal assuming cloudless atmosphere, taking into account the main atmospheric effects (gaseous absorption by water vapour, carbon dioxide, oxygen and ozone; scattering by molecules and aerosols).

Here we compare the efficiency and reliability of two radiometric correction techniques applied to SPOT-5 scenes. The first one provides an absolute correction through the application of the atmospheric model 6S, the other consists of a relative calibration based on the use of PIFs.  Accuracy of each technique is compared through the mean variation in reflectance of selected pseudo-invariant features observed after image normalization. We further address how the type of invariant targets and the number of points used affect the accuracy of the normalization with the PIF approach.

## Study site

The Camargue is a flat delta (maximum terrain elevation = 7 m) located near the Mediterranean Sea experiencing a Mediterranean climate with mild and windy winters and hot and dry summers. Six SPOT-5 scenes were programmed and acquired through funds provided by the Centre National d'Études Spatiales (CNES) in December 2004, March, May, June, July and September 2005 covering all the study area. For all images, the view angle was comprised between - 25º and + 25º (generally around 8º) and the cloud percentage below 20%. The scenes were centred on the Vaccarès lagoon and included some deep sea in their southernmost part (Fig. 1). Landcover consists mainly of agricultural land and natural or semi-natural marshes along with three small towns, three villages and part of an industrial zone.

## Methods

### *The 6S Atmospheric model*

The absolute atmospheric corrections were performed according to the method described in Kergomard (2000) originally applied to the 5S model (Tanré et al., 1990). Digital numbers were first converted to physical values according to the linear transformation:

$$\text{radiance}=DN/G$$

where DN is the Digital Numbers and G the absolute calibration gain of the sensor given by SPOT scene for each band. Geometrical conditions are automatically calculated by 6S based on the date, time, longitude and latitude of the scene. Spectral conditions are estimated based on the type of satellite, the sensor and the band to be corrected. We selected lambertian as type of surface. Atmospheric conditions were estimated from the atmospheric profile, the aerosol model, and the visibility. After an exploratory analysis of the data, we selected "maritime" as aerosol model and "mid latitude summer" as atmospheric profile for all images, independently from the wind direction. Visibility was derived from 6S computer iterations assuming that the reflectance in the SWIR band in clear deep water was equal to zero (Kergomard, 2000). We selected one pixel exhibiting the lowest digital counts located 10 km from the coast in clear and deep sea, and ran the model with different values of visibility until obtaining an atmospheric reflectance equal to the one exhibited by this pixel in the MIR band. These values of visibility were calculated for each image and further integrated in the 6S code for assessing the atmospheric conditions of each date. The images were then corrected with the parameters "xa", "xb" and "xc" given in the 6S User Guide (2006). These parameters represent the ratio of total upward and downward flux in the atmosphere, the path radiance, and the spherical albedo of the atmosphere, respectively. For each pixel in the input image, linearly interpolated values of xa, xb and xc are calculated for the actual view zenith angle of that pixel, and the reflectance is calculated using the formulae:

$$y = xa*(\text{measured radiance})-xb$$

$$\text{atmospherically corrected reflectance} = y/(1+xc*y)$$

***Pseudo-Invariant Features (PIFs)***

The number of PIFs used in radiometric correction studies vary from a few dozens (Eckhart et al. 1990; Schroeder et al., 2006) to several hundreds (Over et al., 2003; Janzen et al., 2006; Galiatsatos et al., 2007). In this study, only four types of invariant features covering at least 2x2 pixels and providing a number of independent replicates sufficient for statistical analyses were available on all images (Fig. 1). These were roofs (n = 24), sand (n = 10), water in abandoned quarry, littoral and deep sea (n = 36), and pine trees (n = 16). These PIFs covered the whole range of brightness of the four bands on the reference scene (Fig. 2). For image normalization, we applied the equation of the linear regression between the digital counts of the PIFs from the reference image and those from the image to be corrected after geometric rectification. We used the December image normalized with the 6S atmospheric model as a reference for comparing the radiometric variation obtained with both approaches.  By doing so we eliminated, rather than levelled off, the atmospheric effects on all images to avoid that the normalized invariant points exhibit a lower variation only due to the systematic loss of signal related to the atmospheric conditions of each image.

***Estimation of radiometric variation***

Radiometric variation was estimated using the 86 points of pseudo-invariant features, except when comparing the PIF and 6S-code techniques. In this latter case, we used half of the PIF points for normalization and the other half for comparison, to avoid biased estimation. The radiometric variation corresponds to the Euclidian distance (Legendre and Legendre, 1998) between the mean radiometric value and the radiometric value at time *j* of each point *i* with the equation:

$$\sum_{i,j} \sqrt{\left(B1_{ij} - \overline{B1}_i\right)^2 + \left(B2_{ij} - \overline{B2}_i\right)^2 + \left(B3_{ij} - \overline{B3}_i\right)^2 + \left(B4_{ij} - \overline{B4}_i\right)^2}$$

where B1, B2, B3 and B4 represent the four spectral bands of SPOT 5. The mean Euclidian distance, which should be theoretically equal to zero if the normalization was perfect and the pseudo-invariant features truly invariant, further provides a radiometric variation that is comparable among points from different types of features or dates. Paired *t*-tests and *t*-tests were used to compare radiometric variation of two series of identical or independent points, respectively. For multiple comparisons, we used ANOVA (F) followed by Scheffe post-hoc tests when statistically significant ($p < 0.05$) (Sokal and Rholf, 1995).

***Comparison of 6S and PIF techniques based on simulations***

Using the radiometric variation of all PIFs, we run 100 permutations with one to ten points from each type of PIF, totalling 1000 permutations. For each set of permutations, we calculated the accuracy of the estimation using the mean radiometric variation with the minimum-maximum range values. The number of PIFs required to reach a radiometric variation comparable to that of 6S was extrapolated from a power curve.

## Results

Overall, normalization using either PIFs (4.0%) or the 6S model (4.3%) provided similar results in radiometric variation (Fig. 3, paired-$t = 1.4$; $df = 43$; $p = 0.17$). However, radiometric variation differed according to the type of features used ($F = 30.9$; $df = 3, 173$; $p < 0.0001$), in a similar way with both normalization techniques ($F = 3.26$; $df = 1, 173$; $p = 0.07$). Deep water and pine trees were the least variant, roofs were more variant with large differences observed among points from the same image, whereas the sand showed the highest variation among dates with the least variation among points from a same date (Fig. 4).

### *Variation in PIF radiometry over time*

Radiometric variation in points from a same type of feature is shown for each scene in figure 5. Although deep water varied little over the year, significant differences occurred among dates ($F = 5.67$; $df = 5; 138$; $p < 0.0001$), with March differing from all other dates except June. The longer confidence interval observed in March and June further suggests a higher variation among points for these two dates. Actually, only the points located in deep sea differed in March (0.151 *vs*. 0.013; $t = -19.58$; $df = 34$; $p < 0.0001$), whereas only the points located in the littoral zone differed in June (0.065 *vs*. 0.018; $t = 5.55$; $df = 34$; $p < 0.0001$). Pine trees also showed a significant radiometric variation across dates ($F = 26.09$; $df$: 5, 108; $p < 0.0001$), with higher values in

December and May, but little variation among points from the same image (Fig. 5). Roofs were the most variable feature ($F = 7.68$; $df = 5, 210$; $p < 0.0001$), with March being significantly different from all other months. The longer confidence intervals observed for all dates are mostly due to the small roofs (mean: 4828 $m^2$, range: 1110 - 12753 $m^2$), which showed a higher radiometric variation than larger roofs (8.6% *vs*. 3.5%; $t = 3.71$; $df = 22$; $p = 0.001$). Sand showed a low radiometric variation except in July and September when values were significantly higher ($F = 7442.21$; $df = 5, 54$; $p < 0.0001$), primarily in the B3 and B4 bands. In spite of these large seasonal differences, very little variation was observed among points from a same date for any date. The withdrawing of the “variant” features (deep water in March and littoral water in June, pine trees in December and May, little roofs, and sand in July and September) allowed to decrease the overall radiometric variation (PIFs = 3.4%; 6S = 2.9%), with the 6S model providing a significantly lower variation (paired-$t = -4.74$; $df = 36$; $p < 0.0001$) than the PIF approach (Fig. 6).

### *Effect of the number of points and features with the PIF technique*

The importance of using several types of PIFs for image normalization is illustrated in figure 7. Using just one type of feature resulted in a significant increase of radiometric variation in all cases ($t$-tests; $p < 0.0001$), with variable results pending upon the type of PIFs used. For instance, reflectance normalization based on roofs only provides the lowest radiometric variation in other features, although roofs were the most variant PIFs. In contrast, reflectance normalization using sand provides the highest radiometric variation in other features, although sand showed the lowest variation among points from a same date. To determine the optimal number of points that should be used for each type of invariant features, we compared the maximal radiometric variation obtained from the permutations with the original radiometric mean (4.0%) used as a threshold value. From this, it appears that five points per PIF types provide a cost-effective estimation of radiometric variation (Fig. 8). However, as many as 31 points per feature would be necessary to provide a radiometric variation that is not significantly different from that obtained with 6S, whereas 292 and 3846 points per feature would be required to provide similar or better results than the 6S code, respectively.

**Discussion and conclusion**

Models for atmospheric corrections generally use a specific language, an unfriendly interface, and require measurements of atmospheric parameters at the time of image acquisition. In contrast, the 6S model is relatively user-friendly and all the information required to perform the corrections are provided with the image with the exception of visibility, which can be deduced from a single pixel of known radiometry. Although we did not use these options, 6S offers the possibility to account for target elevation and to integrate non-lambertian surface conditions, as well as more absorbing species and successive order of scattering (SOS) algorithm, all of which are of particular interest for environmental monitoring (Vermote et al., 1997). Kergomard (2000) selected the aerosol type based on wind direction. However, based on the radiometry of invariant features, 6S provided a better normalization of the Camargue images when the aerosol model was set at maritime even under north-blowing wind conditions. Likewise, selecting a “mid latitude summer” atmospheric profile, even for the December image, provided a better fit for the Camargue, even though Kergomard (2000) found that the atmospheric profiles had a limited impact on his results. Hence, in further 6S applications we recommend testing the effects of different inputs on the radiometric values of a few invariant features to identify the most appropriate atmospheric conditions for each date and region.

Our analyses first revealed a similar accuracy in radiometric normalization using either the 6S code or PIFs. Because PIFs are not totally invariant, and that these variations are taken into account with the PIF but not the 6S approach, radiometric variation was originally slightly lower with the corrections based on PIFs. However, when the most variant PIFs are withdrawn, the 6S model becomes significantly more accurate. The variations observed in the PIFs selected were related to various factors depending upon the type of features. For instance, radiometric variations in the sea are probably related to increased water turbidity through alluvia brought by the Rhone River near the coast and to variation in wave height in deep sea. Radiometric variation in pine trees is probably associated with needle production in June and their drying out in December, whereas those observed with sand are presumably related to their humidity content. Human constructions such as roofs can also be used, but in this study only roofs larger than 15 000 $m^2$ or 12 x 12 pixels were relatively invariant. This study and others (Du et al., 2002; Furby and Campbell, 2001) have demonstrated the importance of using different types of features covering the full range of brigthness. Our results additionally showed that at least five different objects per type of feature should be used. These objects should be selected carefully, as a large number of presumably invariant points were tested preliminarily and eliminated in this study. Yet, systematic variation in all objects of a same feature will be difficult to detect, especially when only two images are being used.

Regardless of the method involved, some radiometric variation remains, which can be due to several factors (Du et al., 2002), including the differing view angles (Moran et al, 1990) and degradation of optical sensor (Bannari et al, 1999) at the satellite level. Additionally, geometric corrections can create residual errors. With the 6S code, using a single reference point on the image can provide inconsistency in radiometry due to a spatial variation of aerosols causing heterogeneous atmospheric effects across the image. Several methods exist to estimate the accuracy of the radiometric normalization, making comparisons difficult (Moran et al., 1992; Chavez, 1996, Heo and FitzHugh, 2000; Song et al., 2001, Schroeder et al., 2006). Du et al. (2002) obtained a mean error of 1.1% by band, which is comparable to our results with 6S (0.7%) and PIFs (1.0%). Although the use of 6S provides more accurate results, this study shows that the use of PIFs remains a valid approach, as long as the invariant targets are selected carefully and empirically tested for their radiometric variation.

**References**

6S User Guide Version 2, November 2006, 218 p. *http://6s.ltdri.org/6S_code2_thiner_stuff/6S_ltdri_org_manual.html*

Bannari A., Teillet P.M., Richardson G., 1999. Nécessité de l'étalonnage radiométrique et standardisation des images numériques de télédétection. Canadian Journal of Remote Sensing, 25: 45-59.

Caselles, V., and M.J. Lopez Garcia, 1989. An alternative simple approach to estimate atmospheric correction in multitemporal studies. International Journal of Remote Sensing, 10:1127-1134.

Chavez P.S.Jr., 1996. Image-based atmospheric corrections revisited and improved. Photogrammetric Engineering and Remote Sensing, 62: 1025-1036.

Du, Y., P.M. Teillet, and J. Cihlar, 2002. Radiometric normalization of multitemporal high-resolution satellite images with quality control for land cover change detection. Remote Sensing of Environment, 82:123–134.

Eckhardt, D.W., J.P. Verdin, and G.R. Lyford, 1990. Automated update of an irrigated lands GIS using SPOT HRV imagery. Photogrammetric Engineering and Remote Sensing, 56:1515-1522.

Furby, S.L. and N.A. Campbell, 2001. Calibrating images from different dates to ‘like-value’ digital counts. Remote Sensing of Environment, 77:186-196.

Galiatsatos, N., D.N.M. Donoghue, D. Knox, and K. Smith. 2007. Radiometric normalisation of multisensor/multitemporal satellite images with quality control for forest change detection. In: Fourth international workshop on the analysis of multi-temporal remote sensing images, Leuven, Belgium.

Heo, J. and T.W. FitzHugh. 2000. A standardized radiometric normalization method for change detection using remotely sensed imagery. Photogrammetric Engineering and Remote Sensing, 66: 173-181.

Janzen, D.T., A.L. Fredeen, R.D. Wheate, 2006. Radiometric correction techniques and accuracy assessment for Landsat TM data in remote forested regions. Can. J. Remote Sensing, Vol. 32, No. 5, pp. 330–340, 2006

Kergomard, C., 2000. Pratique des corrections atmosphériques en télédétection : utilisation du logiciel 5S-PC. Cybergeo, N°. 181. http://www.cybergeo.presse.fr/ teldschu/kergomar/kergomar.htm

Legendre, P. and L. Legendre, 1998. Numerical Ecology. 2nd English edition, Elsevier, Amsterdam, The Netherlands.

Lillesand, T. M. and R.W. Kiefer, 2000. Remote Sensing and Image Interpretation. 4th edition. John Wiley and Sons, Inc., New York, New York.

Mathevet, R. 2004. *Camargue incertaine*. Sciences, usages et natures. Buchet-Chastel, Paris, France. 201 p.

Moran, M.S., R.D. Jackson, G.F Hart, P.N. Slater, R.J. Bartell, S.F. Biggar, D.I. Gellman, and R.P. Santer, 1990. Obtaining surface reflectance factors from atmospheric and view angle corrected SPOT-1 HRV data. Remote Sensing of Environment, 32: 203-214

Moran, M.S., R.D. Jackson, P.N. Slater, and P.M Teillet, 1992. Evaluation of simplified procedures for retrieval of land surface reflectance factors from satellite sensor output. Remote Sensing of Environment, 41:169-84.

Over M., B. Schöttker, M. Braun, G. Menz, 2003. Relative radiometric normalisation of multitemporal Landsat data – A comparison of different approaches. Proc. IGARSS 2003, 21-25 July, Toulouse, France.

Paolini, L., F. Grings, J.A. Sobrino, J. C. Jimenez Muños, and H. Karszenbaum, 2006. Radiometric correction effects in Landsat multi-date/multi-sensor change detection studies. International Journal of Remote Sensing, 27:685-704.

Rahman, H. and G. Dedieu, 1994. SMAC: A Simplified Method for the Atmospheric Correction of satellite measurements in the solar spectrum. International Journal of Remote Sensing, 15:123-143.

Richter, R., 1990. A fast atmospheric correction algorithm applied to Landsat TM images. International Journal of Remote Sensing, 11:159-166.

Schott, J.R. 2007. Remote sensing: the image chain approach. 3rd edition. Oxford University Press, Oxford, UK.

Schott, J.R., C. Salvaggio and W.J. Volchok, 1988. Radiometric image normalization using pseudo-invariant features. Remote Sensing of Environment, 26:1-16.

Schroeder, T.A.; W.B. Cohen, C. Song, M.J. Canty, and Z. Yang, 2006. Radiometric correction of multi-temporal Landsat data for characterization of early successional forest patterns in western Oregon. Remote Sensing of Environment, 103: 16-26.

Sokal, R.R. and F.J. Rholf, 1995. Biometry. WH Freeman, New York.

Song C., C.E. Woodcock, K.S. Seto, M.P. Lenney, and S.A. Macomber. 2001. Classification and change detection using Landsat TM data: when and how to correct atmospheric effects? Remote Sensing of Environment, 75: 230-244.

SPOT Image, 2005. Technical information SPOT, Resolutions and spectral modes, 4 pp.http://www.SPOTimage.fr/automne_modules_files/standard/public/p233_1bbabf31105a2cf49217f6ce79596d0cres_modes_E.pdf

Tamisier, A., and P. Grillas, 1994. A review of habitat changes in the Camargue: An assessment of the effects of the loss of biological diversity on the wintering waterfowl community. Biological Conservation, 70:39-47.

Tanré D., C. Deroo, P. Duhaut, M. Herman, J.J Morcrette, J. Perbos, and P.Y Deschamps, 1990. Description of a computer code to simulate the satellite signal in the solar spectrum: the 5S code. International Journal of Remote Sensing, 11:659-668.

Vermote, E.F., D. Tanré, J.L. Deuzé, M. Herman, and J.J. Morcrette, 1997. Second Simulation of the Satellite Signal in the Solar Spectrum, 6S: an overview. IEEE Transactions on Geosciences and Remote Sensing, 35:675-686.

Figure Captions

**Fig. 1.** SPOT-5 scene showing the location of the pseudoinvariant points.

**Fig.2.** Proportion of pixels across the reflectance range of each band with distinction of those used as pseudoinvariant features (PIFs).

**Fig. 3.** Radiometric variation (% reflectance) of pseudoinvariant features (PIFs) normalized with the 6S atmospheric model and the PIF approaches (mean with 95% confidence interval).

**Fig. 4.** Radiometric variation (% reflectance) for each type of pseudoinvariant feature when normalized with the 6S atmospheric model and the PIF approaches (mean with 95% confidence interval).

**Fig. 5.** Radiometric variation (% reflectance) for each type of pseudoinvariant features over time (mean with 95% confidence interval).

**Fig. 6.** Radiometric variation (% reflectance) of pseudoinvariant features normalized with the 6S atmospheric model and the PIF approaches when the variant features are excluded (mean with 95% confidence interval).

**Fig. 7.** Radiometric variation (% reflectance) when a single feature is used for radiometric normalization (mean with 95% confidence interval).

**Fig. 8.** Mean radiometric variation with minimum-maximum range values according to the number of points used from each type of PIFS based on permutations.

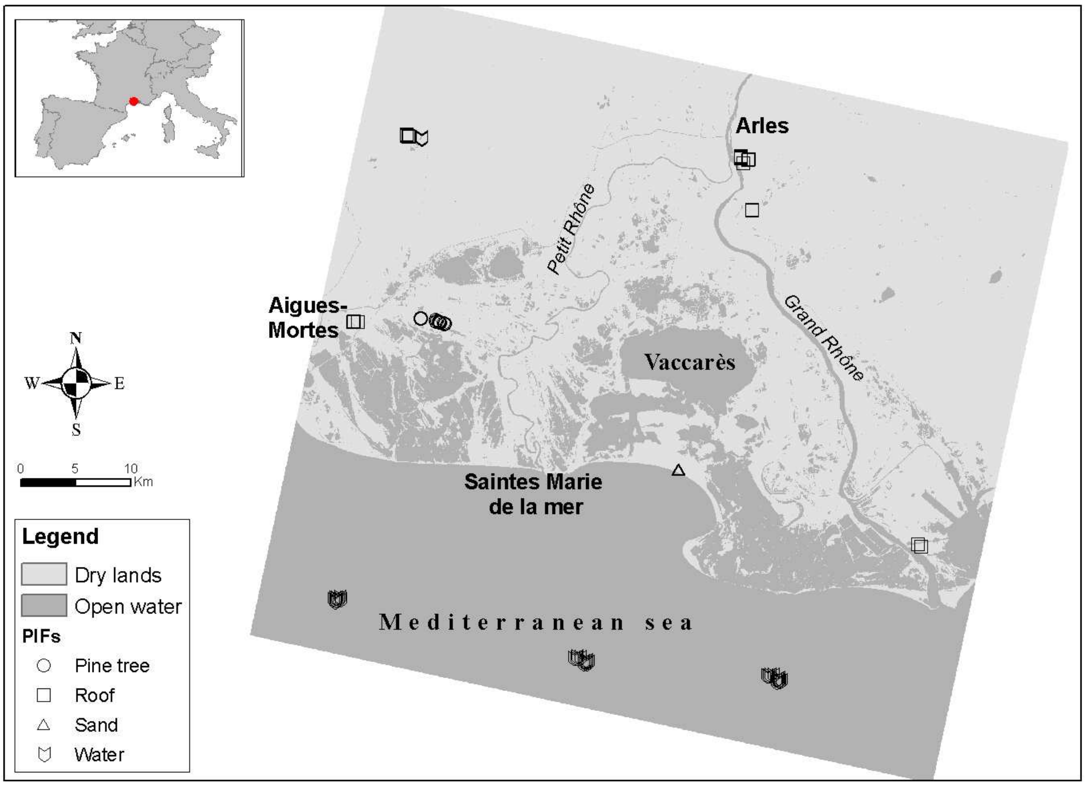

Arles
Petit Rhône
Grand Rhône
Aigues-Mortes
Vaccarès
Saintes Marie de la mer
Mediterranean sea
N
W
E
S
0
5
10
Km
Legend
Dry lands
Open water
PIFs
Pine tree
Roof
Sand
Water

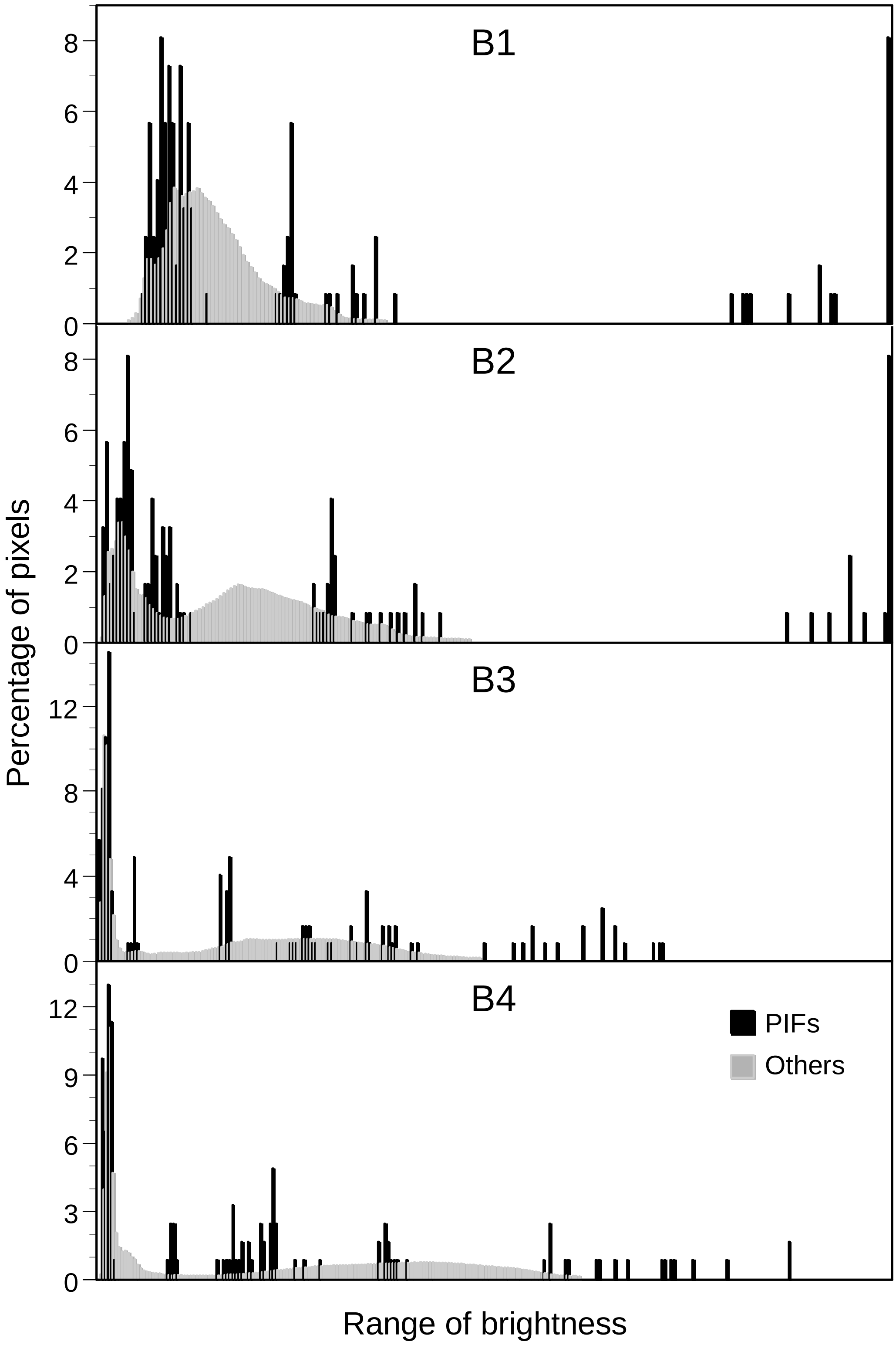
B1
B2
B3
B4
PIFs
Others
Percentage of pixels
Range of brightness
0
2
4
6
8
0
2
4
6
8
0
4
8
12
0
3
6
9
12

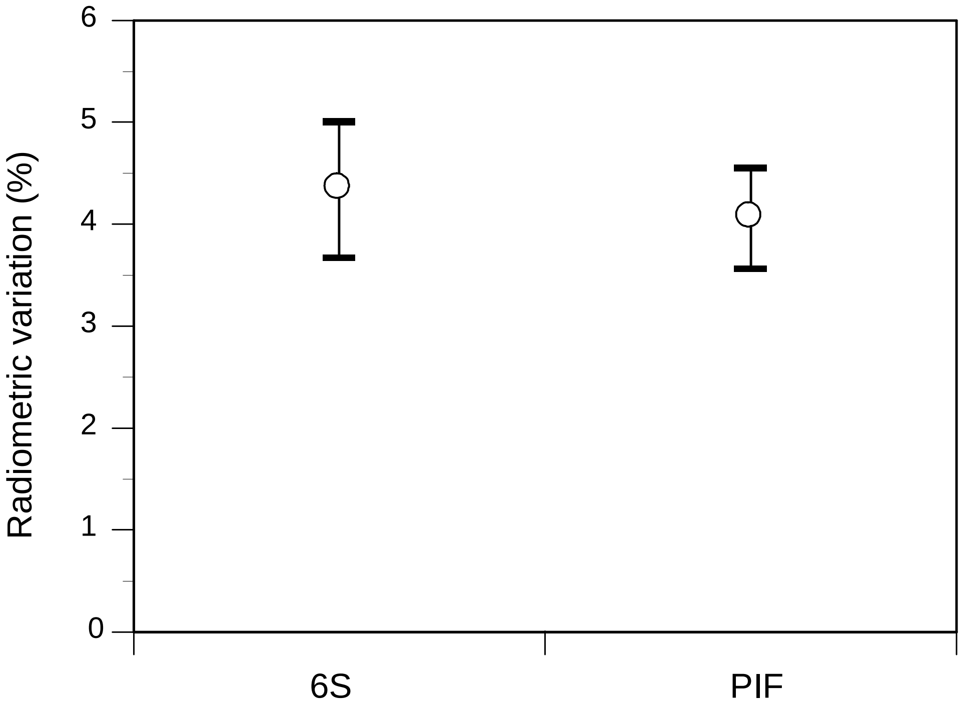

Radiometric variation (%)
0
1
2
3
4
5
6
6S
PIF

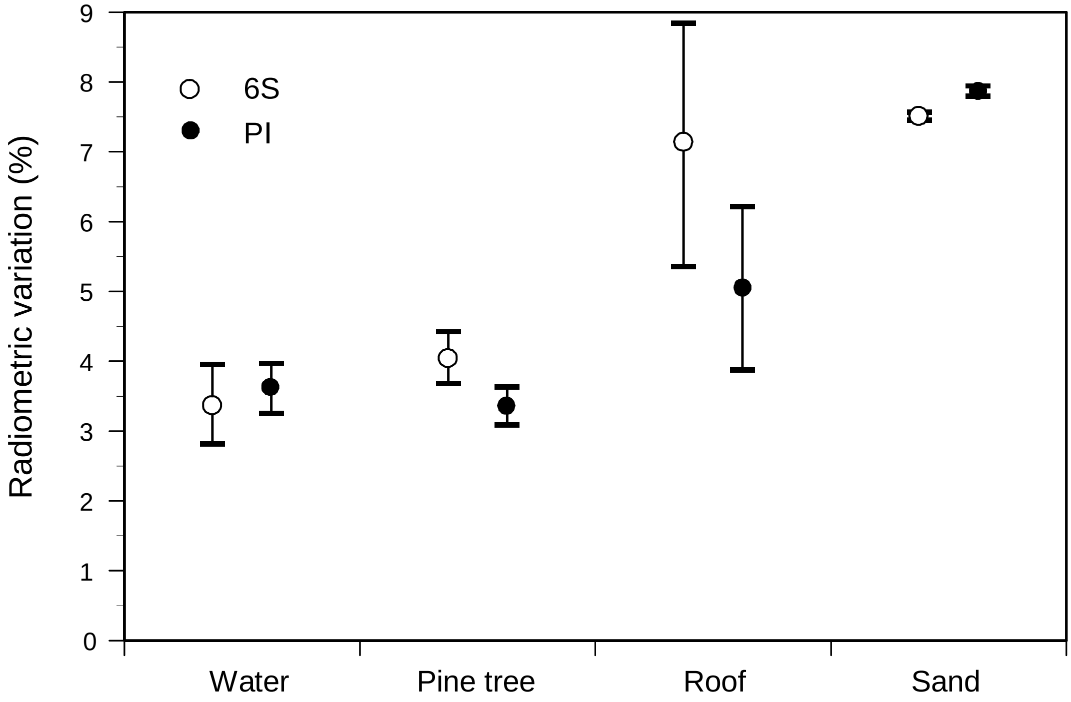
Radiometric variation (%)
9
8
7
6
5
4
3
2
1
0
6S
PI
Water
Pine tree
Roof
Sand

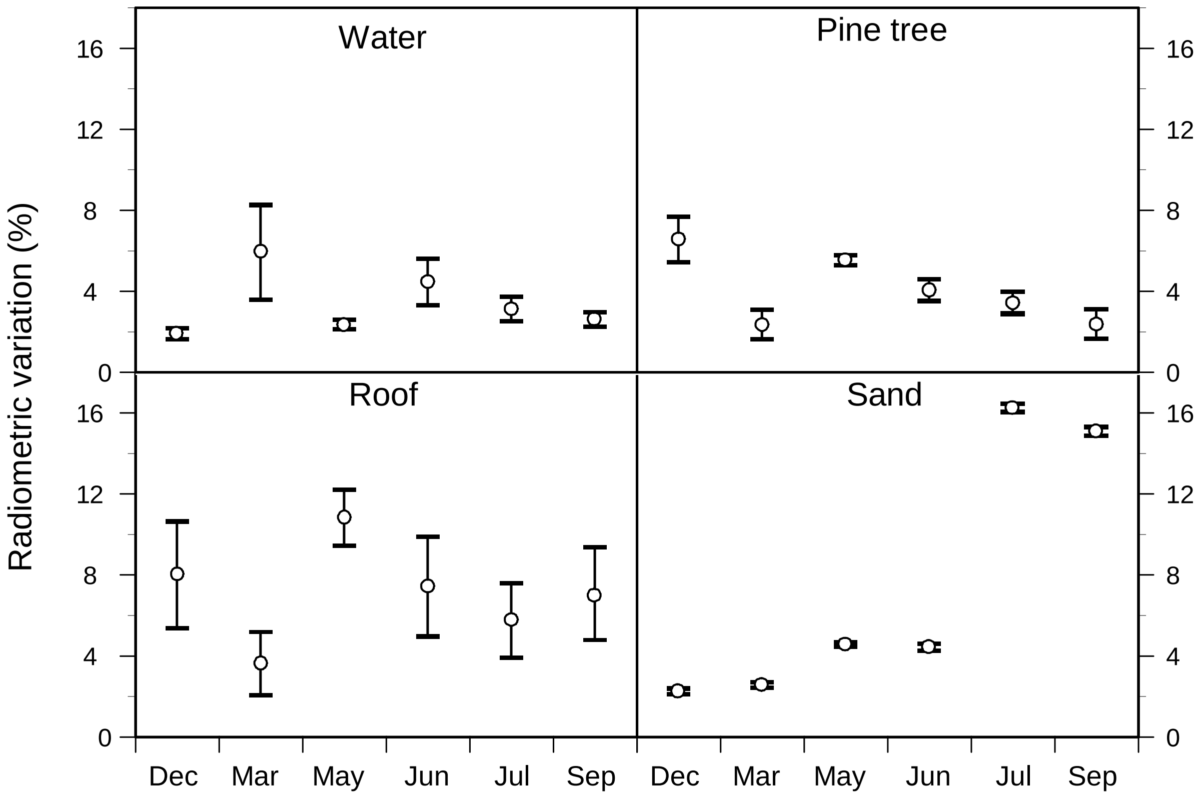
Water
Pine tree
Roof
Sand
Radiometric variation (%)
0
4
8
12
16
Dec
Mar
May
Jun
Jul
Sep

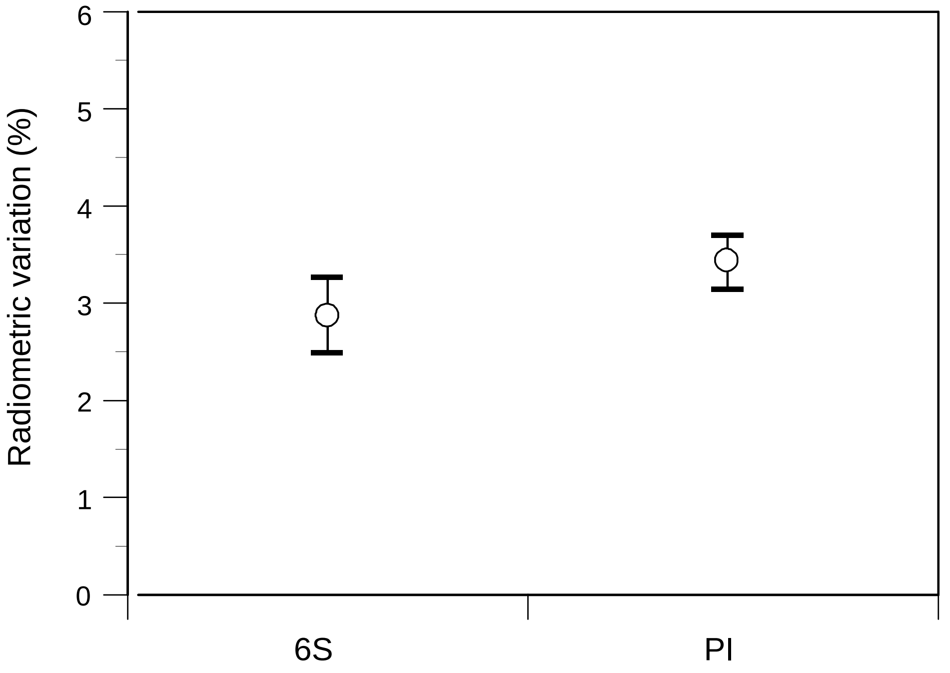
Radiometric variation (%)
0
1
2
3
4
5
6
6S
PI

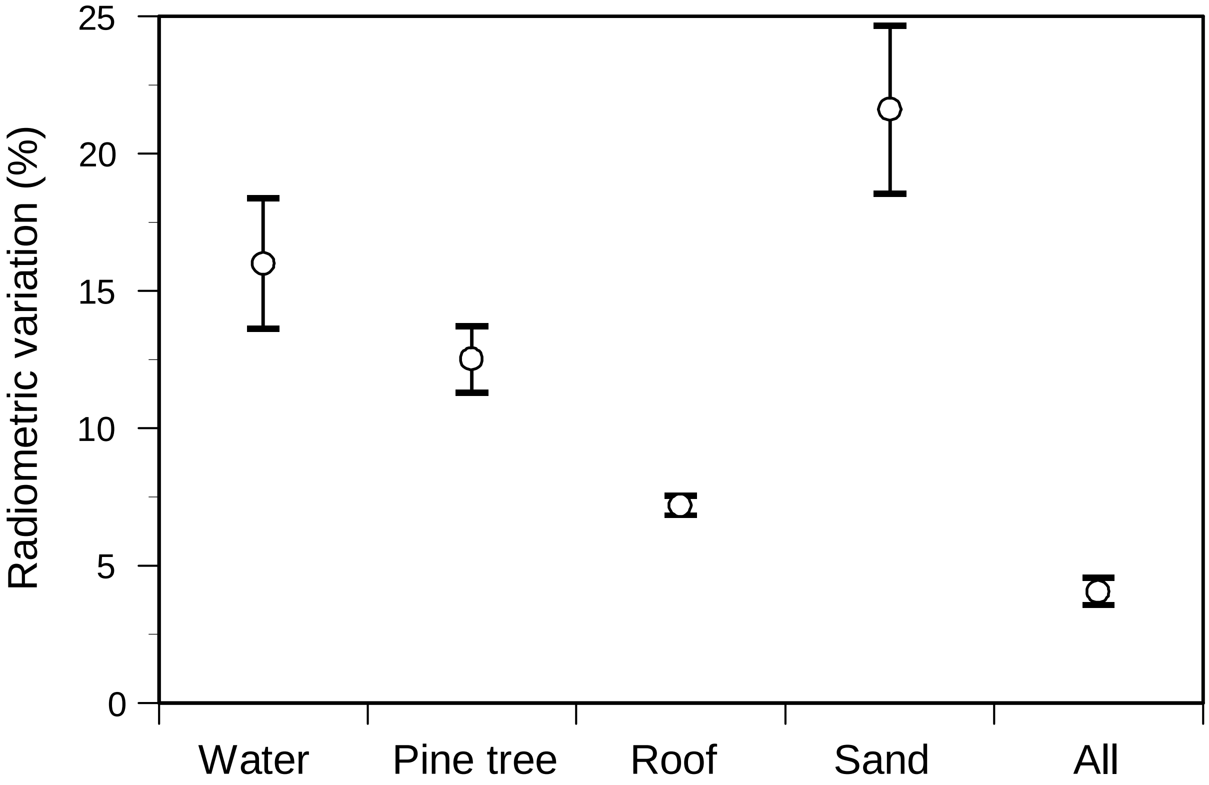

Radiometric variation (%)
0
5
10
15
20
25
Water
Pine tree
Roof
Sand
All

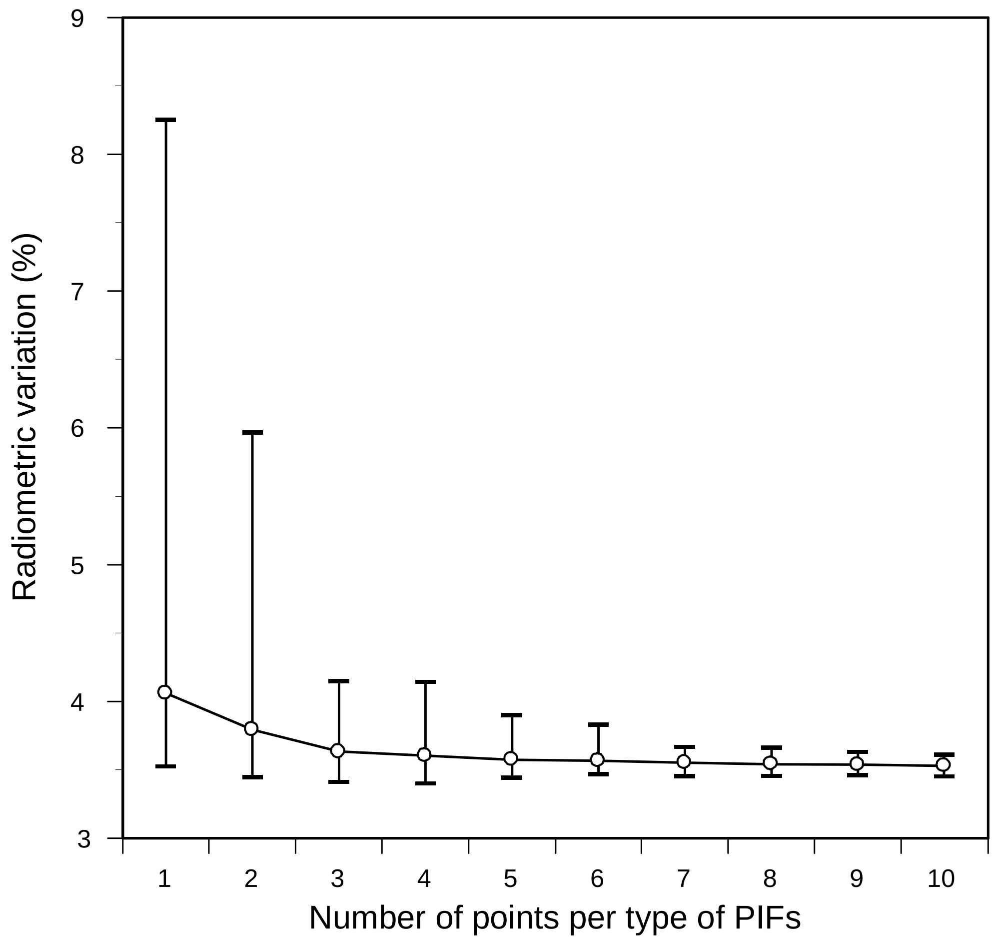
9
8
7
6
5
4
3
Radiometric variation (%)
1
2
3
4
5
6
7
8
9
10
Number of points per type of PIFs